Journal of Power Sources 225 (2013) 286–292

Contents lists available at SciVerse ScienceDirect

Journal of Power Sources

journal homepage: www.elsevier.com/locate/jpowsour

Influence of particle sizes and morphologies on the electrochemical performances of spinel $LiMn_2O_4$ cathode materials

Liang Xiao [a,b,*], Yonglin Guo [a], Deyu Qu [a], Bohua Deng [a], Hanxing Liu [b], Daoping Tang [c]

[a] Department of Chemistry, School of Science, Wuhan University of Technology, Wuhan 430070, Hubei, PR China
[b] State Key Laboratory of Advanced Technology for Materials Synthesis and Processing, Wuhan University of Technology, Wuhan 430070, Hubei, PR China
[c] Shenzhen Herewin Technology Co. Ltd., Shenzhen 518110, Guangdong, PR China

HIGHLIGHTS

- $LiMn_2O_4$ were prepared with accurately controlled morphologies and particle sizes.
- Performances of spherical $LiMn_2O_4$ are better than those of the cubic one.
- Spherical $LiMn_2O_4$ with middle size has the best performance.
- Lithium ion diffusion coefficients of $LiMn_2O_4$ were determined by CITT and PITT.
- Diffusion coefficients depend on morphologies and particle sizes of $LiMn_2O_4$.

ARTICLE INFO

Article history:
Received 5 June 2012
Received in revised form
18 October 2012
Accepted 21 October 2012
Available online 29 October 2012

Keywords:
Spinel $LiMn_2O_4$
Morphology
Particle size
Diffusion coefficient
Spherical particle
Cubic particle

ABSTRACT

Monodispersed and uniform cubic $LiMn_2O_4$ with side length of 5.0 μm denoted as CB and spherical $LiMn_2O_4$ with different diameters (2.0, 3.5, 8.0 μm) denoted as SS, MS, BS respectively are prepared through a controllable precipitation of precursors $MnCO_3$ and a followed melt-impregnation process. Studies show that the electrochemical performance of $LiMn_2O_4$ samples with spherical morphology are better than those of the cubic one. Moreover, the spherical $LiMn_2O_4$ (MS) with middle size (3.5 μm in diameter) has the best electrochemical performance among three spherical samples instead of the smallest spherical $LiMn_2O_4$. The determined apparent lithium ion diffusion coefficients of prepared samples decrease in the order of MS > SS > BS > CB and their values are in the range of $10^{-9.5}$–$10^{-11.5}$ $cm^2\ s^{-1}$ and $10^{-8.0}$–$10^{-10.5}$ $cm^2\ s^{-1}$ from PITT and CITT respectively. This trend matched well with the electrochemical performances of the four cathode materials. This observation can be addressed to the fact that the middle size spherical particles balance the contradictory of diffusion length in solid phase and particle agglomeration, which lead to perfect contacts with the conductive additive, considerable apparent Li-ion diffusion rate and the best performance of MS $LiMn_2O_4$.

1. Introduction

Lithium-ion batteries have attracted widespread interests nowadays with the urgent requirement of advanced chemical power sources for consumer electronic devices, portable power tools, electric vehicles, and so on. The redox reactions in lithium-ion battery are companied with lithium ion insertion into and extraction from the cathode and anode solid phases. As the Li^+ diffusion coefficients are always small in solid phase, the electrode processes of both cathode and anode are restricted by ion diffusion rate. Extensive works have been dedicated to fast ion transportation for improvement of the higher power density of lithium-ion batteries.

One of the strategies to improve the lithium-ion intercalation capacity and rate capability of electrodes is to prepare and use materials with smaller size [1]. Preparations of electrode active materials with nanosize or nanostructure attract extensive interests of electrochemical and material scientists [1–3]. The advantages of electrode material with small size or nanostructure, such as shorter length for both electronic and ionic transport, higher electrode–electrolyte contact area, will facilitate the electrode processes in lithium ion batteries. For example, spinel $LiMn_2O_4$ with theoretical capacity of 148 mAh g^{-1} is a popular cathode material in commercial lithium-ion batteries due to its low cost,

* Corresponding author. Department of Chemistry, School of Science, Wuhan University of Technology, Wuhan 430070, Hubei, PR China. Tel./fax: +86 27 87756662.
E-mail address: leonshaw@yeah.net (L. Xiao).

0378-7753/$ – see front matter © 2012 Elsevier B.V. All rights reserved.
http://dx.doi.org/10.1016/j.jpowsour.2012.10.070

acceptable environmental impact and excellent voltage profile characteristics [4,5]. In order to improve power density of $LiMn_2O_4$ cathode materials, many researchers have fabricated $LiMn_2O_4$ with different nanostructures, including nanowire [6], nanorod [7], hollow spheres [8–10], ordered mesoporous structure [11] and thin-film [12]. These materials with nanostructure and small size make the high current density of lithium ion battery available.

However, scattering results about particle size effects especially in the range of micrometers remains an open question due to the difference in sample preparations and studying methods [13–16]. For instance, Polyakov et al. study the effects of particle size in $LiMn_2O_4$ by mathematical modeling simulation [16]. The $LiMn_2O_4$ samples with different particle sizes were obtained by ball milling the prepared $LiMn_2O_4$ powders in Yi et al.'s study [13]. Yi et al.'s results indicate that $LiMn_2O_4$ with too big or small particle sizes arouse capacity fading, but the initial discharge capacity is only slightly affected. Lu et al. prepared the $LiMn_2O_4$ powder with various range of particle size by using sieves with different sizes and without morphology control [15]. They reported that cathodes consisting of $LiMn_2O_4$ powders with the smaller particle size exhibit the larger capacity and the higher coulomb efficiency.

On the other hand, the particle morphology is a very important factor influencing the electrochemical performances of electrode materials to a very great extent. It has been found that regular spherality of particles could significantly enhance the performances of spinel $LiMn_2O_4$ [17]. Additionally, spherical particles of spinel $LiMn_2O_4$ could lead to high tap density, which affects the energy density of the battery, and uniform surface coating, which is an effective way of enhancing performance [18]. Moreover, several studies from Taniguchi's group suggested that powder properties including crystallite sizes, surface area play significant roles in the electrochemical properties of $LiMn_2O_4$ [19,20]. Better cycle performance of spherical $LiMn_2O_4$ composed of primary nanoparticles can be expected with smaller specific surface area and the larger crystallite size [19]. However, for obtaining good electrochemical performance at high C-rates, the appropriate crystallinity as well as the surface area of the particles needs to be well controlled [20].

In the present work, influences of particle sizes, morphologies and powder properties on the electrochemical performances of spinel $LiMn_2O_4$ cathode materials were comprehensively studied further. Monodispersed and uniform cubic $LiMn_2O_4$ and spherical $LiMn_2O_4$ with different sizes were prepared successfully by a controllable precipitation of precursors $MnCO_3$ derived from literature report [21]. With these accurate controls of morphology and particle size of $LiMn_2O_4$, the crystallite structure, powder property, capacity and rate capability of $LiMn_2O_4$ with different morphologies and particle sizes have been evaluated and compared. Furthermore, in order to explore possible causes for the difference of electrochemical performances of these $LiMn_2O_4$ samples the diffusion coefficients of lithium ion in $LiMn_2O_4$ solid phase have been determined by capacity intermittent titration technique (CITT) and potential intermittent titration technique (PITT).

2. Experimental

2.1. Material preparation and characterization

The $MnCO_3$ precursors were precipitated with manganese sulfate ($MnSO_4$, AR) and ammonium hydrogen carbonate (NH_4HCO_3, AR) according to the literature [21]. 7 mL Ethanol (AR) was added into 70 mL $MnSO_4$ solution with the concentration of 0.0143 mol L^{-1} under stirring. 70 mL NH_4HCO_3 solution with concentration of 0.143 mol L^{-1} was added into the $MnSO_4$-ethanol solution by three times in 25 °C water bath under vigorous stirring. 1/3 of 70 mL NH_4HCO_3 solution was added in each time with the interval time of 30 min. After the addition of all the NH_4HCO_3 solution, the obtained suspension was maintained at 25 °C for 3 h under vigorous stirring. By this route, spherical $MnCO_3$ with the biggest diameter (BS–$MnCO_3$) was prepared. Spherical $MnCO_3$ with the middle diameter (MS–$MnCO_3$) was prepared by rising water bath temperature to 40 °C and keeping other conditions remain unchanged. Comparing to the preparation of MS-$MnCO_3$, spherical $MnCO_3$ with the smallest diameter (SS–$MnCO_3$) was prepared by rising concentration of NH_4HCO_3 solution to 0.286 mol L^{-1} and keeping other conditions remain unchanged. In the preparation of Cubic $MnCO_3$, 10 mmol ammonium sulfate ($(NH_4)_2SO_4$, AR) was added to the 70 mL NH_4HCO_3 solution with the concentration of 0.0143 mol L^{-1}. Then, all the NH_4HCO_3–$(NH_4)_2SO_4$ solution was rapidly added into the above mentioned $MnSO_4$–ethanol mixture. After a following aging in 50 °C water bath for 5 h without stirring, cubic $MnCO_3$ particles were prepared. All the $MnCO_3$ precursors were separated from the reaction mixture by centrifugation, and then washed several times with deionized water and ethanol to remove impurities. Finally, all the $MnCO_3$ precursors were dried at 40 °C in a vacuum oven for 3 h before using.

The $LiMn_2O_4$ cathode materials with spinel structure were synthesized through melt-impregnation process [22]. The $MnCO_3$ precursors were decomposed at 560 °C for 4 h to get Mn_2O_3 intermediate at first [23]. Then, the Mn_2O_3 intermediate and $LiOH \cdot H_2O$ (AR) were mixed thoroughly with Li/Mn atomic ratio of 1.05:2. After thorough mixing and grounding in a mortar, the mixture was preheated to 480 °C (melting point of $LiOH \cdot H_2O$) for 6 h in air. Then, the mixture was heated to 750 °C fast within 1 h and was holding at 750 °C for 12 h. Finally, the as-prepared samples were cooled by exposing them to air at room temperature directly.

Structure characterization of the as-prepared $LiMn_2O_4$ samples were performed by X-ray diffractometer (XRD, Rigaku D/MAX-III) with Cu Kα radiation (λ = 1.54056 Å). Data were collected in the 2θ range 10°–80° with a scan rate of 2°/min to obtain the diffraction patterns. The morphologies of the $MnCO_3$ precursors and the final $LiMn_2O_4$ samples were observed by scanning electron microscopy (SEM, JSM-5610LV). The chemical composition of as-prepared powders was checked by inductively coupled plasma spectroscopy (ICP-AES, Iris Intrepid II). The surface area of powders was determined by BET method using nitrogen (Micromeritics Tristar 3000 analyzer).

2.2. Electrochemical performance and diffusion coefficient

2032 coin cells were assembled to test the electrochemical performances of as-prepared $LiMn_2O_4$ Samples. To prepare the electrode, the active $LiMn_2O_4$ materials were mixed thoroughly with conducting acetylene black and Polyvinylidene Fluoride (PVDF) binder with the weight ratio of 85:10:5 in N-methyl-2-pyrrolidone (NMP) solvent to form slurry. Then the slurry was coated on stainless steel substrate and dried at 120 °C in a vacuum oven for 12 h. Electrochemical cells were assembled in Ar-filled glove box with metallic lithium foil as the counter electrode, Celgard 2321 triple-layer polypropylene-based membrane as the separator, and 1 mol L^{-1} $LiPF_6$ in 50%–50% ethyl carbonate (EC) and dimethyl carbonate (DMC) as the electrolyte. All the electrochemical studies were carried out on NEWARE BTS battery tester at room temperature and all potential refer to Li^+/Li.

The galvanostatic charge/discharge experiments were performed between 3.5 and 4.3 V at different current densities. 0.1 C means a current density of 14.8 mA g^{-1}. To find the possible reason for the difference of specific capacities and rate capabilities of different samples, potential intermittent titration technique (PITT)

[24] and capacity intermittent titration technique (CITT) [25] were used to determine the chemical diffusion coefficient of lithium ion in $LiMn_2O_4$ cathodes. The cell was charged and discharged for the several cycles between 3.5 and 4.3 V at 0.1 C before each test. PITT tests are comprised with multiple continuous potential steps in the potential range of 3.5–4.3 V with appropriate amplitude. In each step, the cell was hold at an initial potential for 24 h to make sure the equilibrium state reached. Then the potential was stepped to end potential until the current decreased to less than 1% of the maximum current of this step. In the CITT procedure, the cells were charged with constant current at 0.1 C from an initial potential to a cutoff potential, then the cells were charged with constant potential at this cutoff potential until the current tends to zero (0.005 mA).

3. Results and discussion

3.1. Morphologies and structures

Fig. 1 shows the SEM images of the $MnCO_3$ precursors and the corresponding $LiMn_2O_4$ products. By controlling the precipitation conditions, uniform and monodispersed spherical $MnCO_3$ with different diameters and cubic $MnCO_3$ were prepared as shown in Fig. 1a–d. To facilitate discussions, the spherical $MnCO_3$ precursors with diameters of 2.3 μm, 3.8 μm, 9.0 μm and the cubic $MnCO_3$ precursors with side length of 6.6 μm were signed as SS–$MnCO_3$, MS–$MnCO_3$, BS–$MnCO_3$ and CB–$MnCO_3$, respectively. It is noted that the morphologies of the $MnCO_3$ precursors were inherited by the final $LiMn_2O_4$ products. Consequently, we mark the spherical $LiMn_2O_4$ with diameters of 2.0 μm, 3.5 μm, 8.0 μm as SS–$LiMn_2O_4$, MS–$LiMn_2O_4$, BS–$LiMn_2O_4$ and the cubic $LiMn_2O_4$ with side length of 5.0 μm as CB–$LiMn_2O_4$ respectively. As-prepared $LiMn_2O_4$ including spherical and cubic samples are porous particles agglomerated with small crystalline grains instead of the smooth surface of $MnCO_3$ precursors, and are smaller than $MnCO_3$ precursors. The porous structure and the shrink of as-prepared $LiMn_2O_4$ are attributed to the CO_2 evolution from $MnCO_3$ bulk during the thermal decomposition of $MnCO_3$ to form manganese oxide.

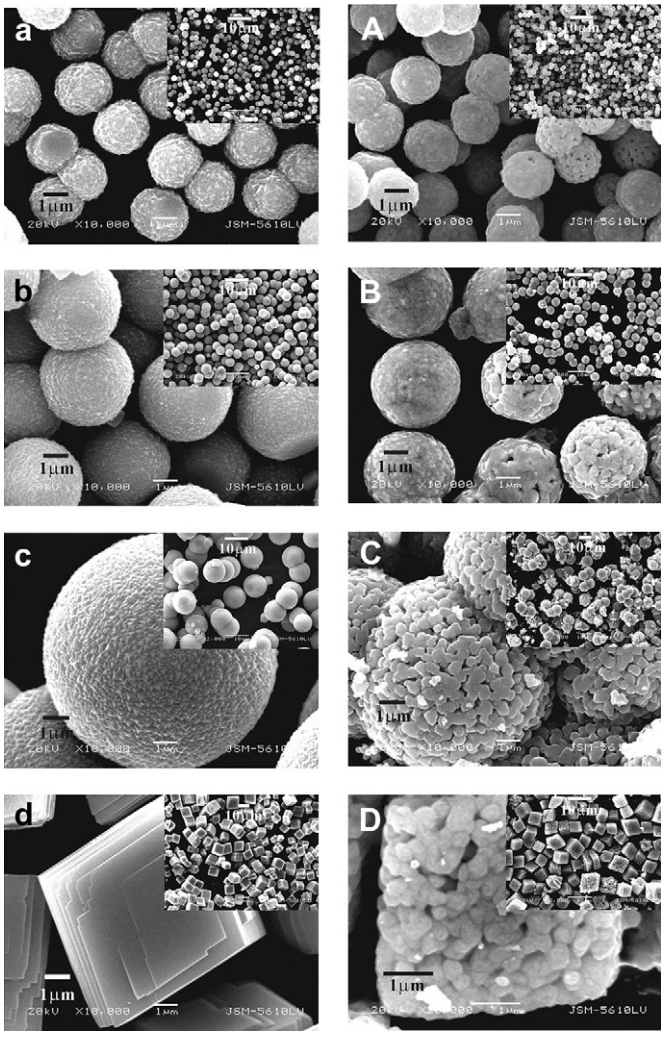

Fig. 1. SEM images of (a) SS $MnCO_3$, (b) MS $MnCO_3$, (c) BS $MnCO_3$, (d) CB $MnCO_3$ and (A) SS $LiMn_2O_4$, (B) MS $LiMn_2O_4$, (C) BS $LiMn_2O_4$, (D) CB $LiMn_2O_4$.

X-ray diffraction (XRD) patterns of the four $LiMn_2O_4$ samples are shown in Fig. 2. The XRD patterns of all the four samples are in agreement with the standard pattern of spinel $LiMn_2O_4$ and previous report [10]. All the four samples were identified as a single pure phase of cubic spinel structure in the space group Fd-3m, in which the lithium ions occupy the tetrahedral (8a) sites and manganese metal ions reside at the octahedral (16d) site. Size of crystal grains were calculated by Scherrer equation $D = K\lambda/\beta\cos\theta$ based on the lattice plane (111), where the value of Scherrer constant K is 0.89, λ is the X-ray wavelength (0.1541 nm) for Cu K_α, β (radian) is the full width at half maximum (FWHM) of the peak (111) and θ is the angle of diffraction peak. The crystal grain sizes are 36.0, 43.6, 50.4 and 48.5 nm for SS, MS, BS and CB $LiMn_2O_4$ respectively. The macro particles agglomerated with nano sized crystalline grains were also confirmed by SEM. The particle properties of as-prepared particles are summarized in Table 1. Except for the crystallite size and specific surface area, the chemical compositions of samples were quite similar. It is observed that the size of crystal grains increase and the specific surface area decrease with the increasing of the particle sizes of four $LiMn_2O_4$ samples.

3.2. Electrochemical performances

Coin-type cells were used to evaluate the relationship between the electrochemical performances and the morphologies together with the particle sizes. The $LiMn_2O_4$ materials with different

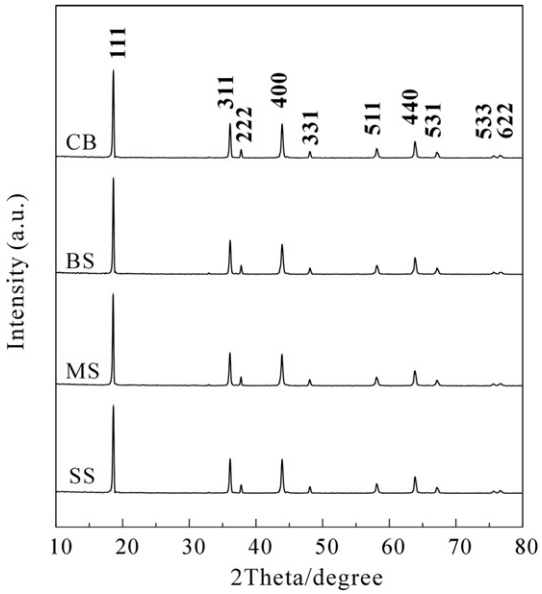

Fig. 2. XRD patterns of prepared $LiMn_2O_4$.

Table 1
Particle properties of as-prepared $LiMn_2O_4$ samples.

Morphology	Particle size (μm)	Crystallite size (nm)	Chemical composition			Specific surface area (m^2/g)
			Li	Mn	O	
SS	2.0	36.0	0.998	2.019	4	4.30
MS	3.5	43.6	0.997	2.008	4	4.15
BS	8.0	50.4	0.994	1.998	4	3.92
CB	5.0	48.5	0.996	2.013	4	4.03

morphologies and particle sizes were used as cathode materials. Fig. 3 shows the first charge and discharge profiles of these materials at 0.1 C rate (14.8 mA g^{-1}) at room temperature. There were two obvious potential plateaus at around 4.00 and 4.15 V for both the charge and discharge curves, which is the typical electrochemical behavior of spinel $LiMn_2O_4$ with phase transformation. One of the acceptable views for such phenomenon is that the appearance of the higher plateau at 4.15 V might exist because of the phase transformation between λ-Mn_2O_4 and $Li_{0.5}Mn_2O_4$, while the lower plateau at 4.00 V is due to the phase transformation between $Li_{0.5}Mn_2O_4$ and $LiMn_2O_4$ [26]. The first charge specific capacities were found to be 143.9, 146.5, 144.3 and 138.0 mAh g^{-1}, and the first discharge specific capacities were 134.9, 136.6, 134.2 and 130.0 mAh g^{-1} for SS, MS, BS, and CB $LiMn_2O_4$, respectively. It shows that all the capacities of $LiMn_2O_4$ samples with spherical morphology are higher than that of the cubic one. And, the spherical $LiMn_2O_4$ sample with diameter of 3.5 μm (MS) has the highest specific capacity. It should be noted that the performance difference among MS, SS, BS and CB is limited in small value. However, the performance of each sample was evaluated more than 24 times in this study. The specific charge/discharge capacities are in normal distribution and the deviations are in the range of ±5 mAh g^{-1}. The selected performance values are the intermediate values in the normal distributions. From this point of view, the variation trend of performances of four samples has good reproducibility.

The cycle performances of the four $LiMn_2O_4$ materials were tested between potential 3.5 and 4.3 V at the 0.1 C rate (Fig. 4). The discharge capacities of the four samples remained 119.4(SS), 122.9(MS), 115.9(BS), 105.1(CB) mAh g^{-1} after 50 cycles. It was noticed that the MS $LiMn_2O_4$ has the best cycle performance. The rate capability, especially at high power demand, is another important aspect for the application of manganese-based spinel cathodes for EV/HEV besides the cycle performance [27]. Fig. 5 displays the discharge capacities at different rates ranging from

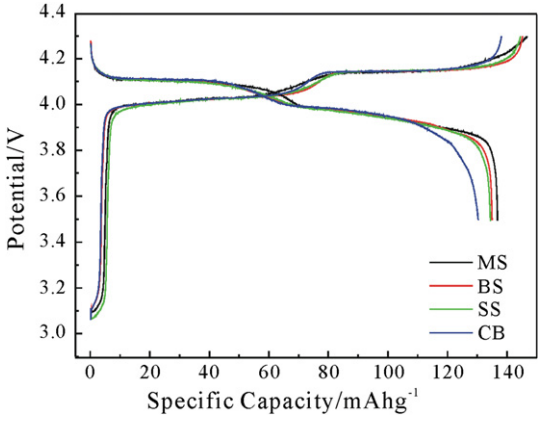

Fig. 3. The first charge and discharge profiles of $LiMn_2O_4$ samples (SS, MS, BS and CB) at 0.1 C.

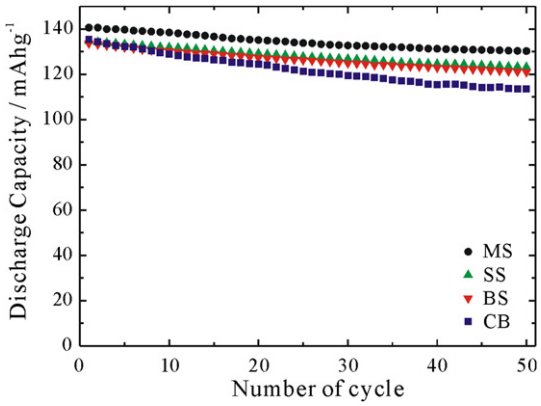

Fig. 4. Cycle performances of $LiMn_2O_4$ samples (SS, MS, BS and CB) at 0.1 C between 3.5 and 4.3 V.

0.5 C (74 mA g^{-1}) to 10 C (1480 mA g^{-1}). The MS $LiMn_2O_4$ was also found to have the best rate performance which approaches to the level of nano-$LiMn_2O_4$ cathode materials [6,7,28]. To investigate the influence of high current density cycles on the electrode materials, the cells were tested again at 1 C rate following above mentioned high rate measurements. The discharge retention rates for MS $LiMn_2O_4$, SS $LiMn_2O_4$, BS $LiMn_2O_4$ and CB $LiMn_2O_4$ electrodes were respectively 98.1%, 97.1%, 97.2% and 94.1% of its initial discharge capacity at 1 C rate, which indicate the high reversibility of the cathode materials.

The present work showed that all the three spherical $LiMn_2O_4$ samples have better performance in both capacity and rate capability than the cubic one. It is in agreement with the results in the literature that regular sphericity of particles could significantly enhance the performance of spinel $LiMn_2O_4$ [17]. Powder materials composed of spherical particles have higher mobility than that of irregular particles. This mobility will facilitate the uniform mix of electrode materials and conductive agent to decrease the resistance of electrode. In the other hand, one of the believed strategies to improve the lithium-ion intercalation capacity and rate capability of electrodes is downsizing from conventional bulk state to nano-scale dimension. Electrode materials with smaller sizes have shorter length for both electronic and ionic transport, which will lead to better electrochemical performance. However, in this study, spherical $LiMn_2O_4$ with the best performance were found to be the one with middle size. To study this uncommon observation, lithium ion diffusion coefficient of prepared samples as an important kinetic parameter related to electrochemical performance were investigated by potential intermittent titration technique (PITT) and capacity intermittent titration technique (CITT).

3.3. Determination of diffusion coefficients

It is generally believed that the charge and discharge of $LiMn_2O_4$ were governed by the diffusion of lithium ion in solid phase. In PITT experiments, a small potential step (50 mV) and a long enough time were adopted to ensure the equilibrium states were reached at every potential step. A plane diffusion model was used without the consideration of charge transfer resistance. The diffusion coefficient determined and discussed in the following paragraph should be taken as an apparent diffusion coefficient (D_{app}).

According to the equations for the diffusion into or out from plane in long time domain of finite diffusion, the current response $i(t)$ in potential step decreases exponentially with time to a good approximation [29]:

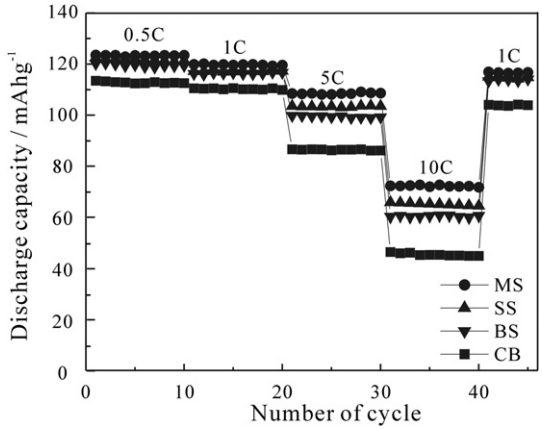

Fig. 5. Rate performances of $LiMn_2O_4$ samples (SS, MS, BS and CB) between 3.5 and 4.3 V.

$$i(t) = \frac{2nFAD\Delta C}{L}\exp\frac{-\pi^2 Dt}{4L^2} \quad (1)$$

where F is the Faraday constant, L is the thickness of the electrode, ΔC is the variation of the surface concentration caused by the potential step for lithium ion, n is the number of electrons and $n = 1$ for the redox of $LiMn_2O_4$. Equation (1) in logarithmic form is:

$$\ln i(t) = \ln\frac{2nFAD\Delta C}{L} - \frac{\pi^2 D}{4L^2}t \quad (2)$$

Equation (2) shows a linear relationship between logarithm of current response of plane electrode and time. Fig. 6 shows a good linearity predicated by Equation (2) which was obtained beyond 2000 s after the potential step. Diffusion coefficient of lithium ion can be calculated by slope of Equation (2) and the knowledge of thickness of $LiMn_2O_4$ electrode measured by micrometer calipers.

The values of apparent diffusion coefficient measured from PITT plotted with various end potential were shown in Fig. 7. These diffusion coefficient values varied from $10^{-9.5}$ to $10^{-11.5}$ cm^2 s^{-1} which matched well with the previous result [30]. There are two minimum peaks at around 4.00 V and 4.15 V respectively in all the diffusion coefficient–potential profiles, and the two peaks make curves a regular "W" shape. The diffusion coefficients of different samples decreased in the following order: MS > SS > BS > CB.

To estimate the variation of diffusion coefficient during charge/discharge cycles, capacity intermittent titration technique (CITT)

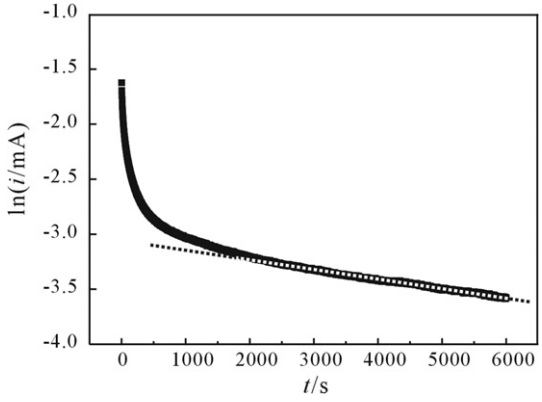

Fig. 6. A typical current response of MS $LiMn_2O_4$ electrode with thickness of 73 μm under potential step from 4.15 V to 4.20 V.

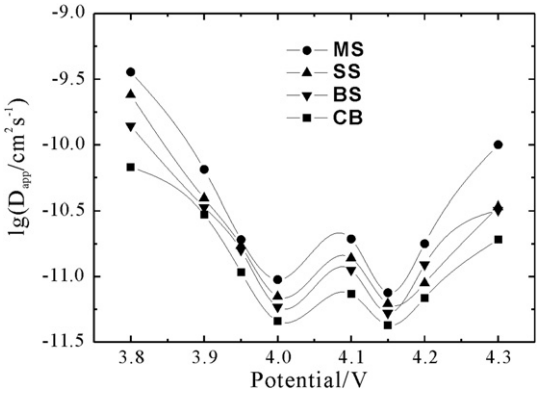

Fig. 7. Diffusion coefficients of $LiMn_2O_4$ samples (SS, MS, BS and CB) calculated from PITT.

were used to determine lithium ion diffusion coefficient of three spherical samples (SS, MS, BS) after different cycles according to the literature [25]. The capacity intermittent titration technique (CITT) based on the ratio of the potentio-charge capacity (Q_p) to the galvano-charge capacity (Q_G) (RPG method). It only needs one complementary parameter (the radius of insertion-host particle R) of the material. Meanwhile, it is just useful for spherical diffusion in spherical particles. The value of t_G (galvano-charge times) in every galvano-potentio charge step can be obtained from the curve of current versus time, and the q is the ratio of the galvano-charge capacity and the potentio-charge capacity for every galvano-potentio charge step. With the parameters of R, t_G and q, the diffusion coefficients can be calculated by selecting a corresponding equations according to Tang's works [25]. Typical CITT curves with a galvano-charge current are shown in Fig. 8. The details of CITT results for $LiMn_2O_4$ are given in Table 2.

The diffusion coefficient of three spherical $LiMn_2O_4$ after different cycles, calculated from CITT, were plotted with potential and shown in Fig. 9. The diffusion coefficient determined by CITT also should be taken as an apparent diffusion coefficient (D_{app}) without the consideration of charge transfer resistance. There are two minimum peaks at around 4.00 V and 4.15 V which make all the curves a regular "W" shape similar to the results from PITT. The diffusion coefficients of different samples also decrease in the same order as those from PITT. Additionally, it should note that charge/discharge cycles promote the diffusion coefficients of all three spherical $LiMn_2O_4$ samples especially at relatively lower rate cycles. This observation is in good agreement with previous studies that

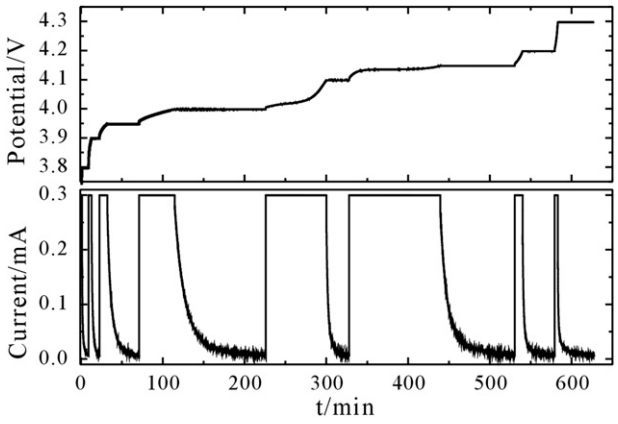

Fig. 8. CITT curves of MS $LiMn_2O_4$ with galvano-charge current of 0.3 mA.

Table 2
Typical data of CITT for MS $LiMn_2O_4$ and the values of diffusion coefficient with corresponding equations.

Potential (V)	Q_G (mAh g^{-1})	Q_P (mAh g^{-1})	t_G (s)	q	Range of q	Equation	$D \times 10^{10}$ (cm^2 s^{-1})
3.8	0.36	0.56	74	1.56	1.51–2.28	$D = \frac{2.75 \times 10^{-2} R^2}{(q-0.65)t_G}$	16.3
3.9	1.13	1.19	218	1.05	0.82–1.51	$D = \frac{3.73 \times 10^{-2} R^2}{(q-0.33)t_G}$	9.5
3.95	3.03	4.16	586	1.37	0.82–1.51		2.4
4.0	13.5	14.3	2614	0.94	0.82–1.51		0.9
4.1	31.3	4.0	4458	0.13	0.06–0.51	$D = \frac{R^2}{15.3 q t_G}$	4.5
4.15	37.5	19.5	6688	0.52	0.51–0.82		0.7
4.2	3.6	2.4	580	0.66	0.51–0.82	$D = \frac{5.15 \times 10^{-2} R^2}{(q-0.10)t_G}$	6.3
l4.3	1.5	1.4	232	0.93	0.82–1.51	$D = \frac{3.73 \times 10^{-2} R^2}{(q-0.33)t_G}$	10.7

values of diffusion coefficient of lithium ion in $LiMn_2O_4$ solid phase tend to increase with the cycling numbers [30]. The high current density cycles may destroyed the crystalline structure and the fragment may hinder the Li^+ diffusion channels, causing the diffusion coefficient of the materials after high rate cycles (Fig. 9B) are smaller than that after low rate cycles (Fig. 9C). The range of diffusion coefficient calculated from CITT were within a range of $10^{-8.0}$–$10^{-10.5}$ cm^2 s^{-1} between 3.80 and 4.30 V, which are almost an order of magnitude higher than the values calculated from PITT.

Although there is variation of diffusion coefficients determined from different techniques due to their different nature, a basic feature can be verified, that the diffusion coefficients of prepared four samples decrease in the order of MS > SS > BS > CB. This trend matched well with the electrochemical performances of the four cathode materials.

3.4. Powder properties and apparent diffusion coefficients

It has already well known that the electrochemical properties of $LiMn_2O_4$ are strongly affected by the chemical composition [31] and powder properties [19]. The chemical compositions of prepared four samples are quite similar (Table 1). Matsuda et al. confirmed that the capacity of $LiMn_2O_4$ increases with the crystallite size of particles and decreases with the specific surface area at the same morphology and size of the particles [19]. In present work, the BS–$LiMn_2O_4$ with the largest crystallite size and the smallest surface area exhibits less capacity than MS–$LiMn_2O_4$. Matsuda et al.'s result is definitely the truth, but it established depend on the morphology and size of the particles being the same. The difference of electrochemical performances of four $LiMn_2O_4$ samples might attribute to the different morphologies and sizes of these samples.

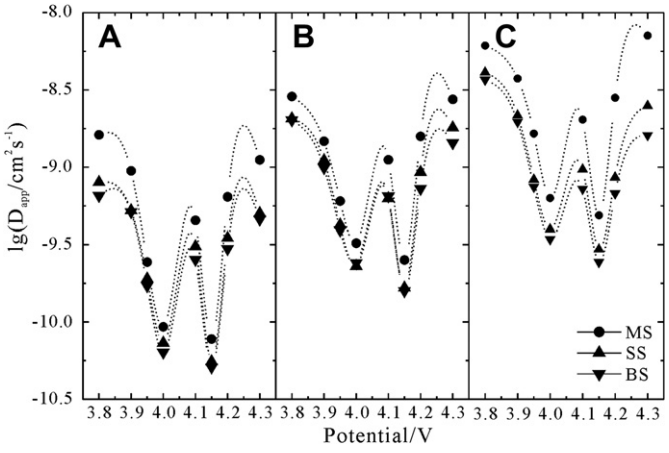

Fig. 9. Diffusion coefficients of $LiMn_2O_4$ samples (SS, MS, BS and CB) after different cycles calculated from CITT, (A) the first cycle, (B) after 45 cycles at high rate as Fig. 5, (C) after 50 cycles at 0.1 C.

It should be noted that the diffusion coefficient determined by both CITT and PITT are apparent diffusion coefficient (D_{app}) without the consideration of particle interior structure, particle surface structure and charge transfer resistance of composite electrode. Bigger apparent diffusion coefficient values should be expected for $LiMn_2O_4$ with smaller crystallite size taking the whole macro particle or electrode into account in calculation [32]. However, it is also not the case in present study. The determined apparent diffusion coefficients of BS–$LiMn_2O_4$ with the largest crystallite size and SS–$LiMn_2O_4$ with the smallest crystallite size are less than that of MS–$LiMn_2O_4$. The relationship of charge transfer resistance of composite electrode and particle morphology and size might play the key role.

The cubic $LiMn_2O_4$ particle is difficult to contact totally with conductive agent due to its less mobility. It is reasonable that the cubic $LiMn_2O_4$ sample has smaller apparent diffusion coefficient and worse performance than the three spherical samples due to the larger charge transfer resistance of cubic $LiMn_2O_4$ composite electrode. For the three spherical $LiMn_2O_4$ samples, the best performance is given by the sample with middle size instead of that with smallest size. This phenomenon can be addressed to the fact that the middle size spherical particles balance the contradictory of Li-ion diffusion rate in solid phase and particle agglomeration. $LiMn_2O_4$ sample with smaller sizes have shorter length for both electronic and ionic transport, which will lead to bigger lithium ion diffusion coefficient and better electrochemical performance. However, the smallest particles are easy to agglomerate, which lead to less contact with conductive. So the largest apparent diffusion coefficient and best performance can be expected for electrode made of spherical $LiMn_2O_4$ particles with moderate particle size.

4. Conclusion

Monodispersed and uniform cubic $LiMn_2O_4$ (CB) with side length of 5.0 μm and spherical $LiMn_2O_4$ (SS, MS, BS) with different diameters (2.0, 3.5, 8.0 μm) can be prepared by a controllable precipitation of precursors $MnCO_3$ and a followed melt-impregnation process. The morphologies of the $MnCO_3$ precursors were inherited by the final $LiMn_2O_4$ products. All the products were well identified as a single pure phase of spinel structure by XRD patterns. Both the specific capacities and the rate capabilities of all the $LiMn_2O_4$ samples with spherical morphology are higher than those of the cubic one. The spherical $LiMn_2O_4$ (MS) with middle size (3.5 μm in diameter) has the best electrochemical performance among three spherical samples instead of the smallest spherical $LiMn_2O_4$. The determined apparent lithium ion diffusion

coefficients of prepared samples decrease in the order of MS > SS > BS > CB and their values are in the range of $10^{-9.5}$–$10^{-11.5}$ cm^2 s^{-1} and $10^{-8.0}$–$10^{-10.5}$ cm^2 s^{-1} from PITT and CITT respectively. This trend matched well with the electrochemical performances of the four cathode materials. This observation can be addressed to the fact that the middle size spherical particles balance the contradictory of diffusion length in solid phase and particle agglomeration, which lead to perfect contacts with the conductive additive, considerable apparent Li-ion diffusion rate and the best capacity of MS $LiMn_2O_4$.

Acknowledgment

This work was supported by the National Natural Science Foundation of China (No. 20803056) and the Fundamental Research Funds for the Central Universities (No. 2010-Ia-013; No. 2012-Ia-039).

References

[1] A.S. Arico, P. Bruce, B. Scrosati, J.M. Tarascon, W. Van Schalkwijk, Nat. Mater. 4 (2005) 366–377.
[2] P.G. Bruce, B. Scrosati, J.M. Tarascon, Angew. Chem.-Int. Edit. 47 (2008) 2930–2946.
[3] Y.G. Wang, H.Q. Li, P. He, E. Hosono, H.S. Zhou, Nanoscale 2 (2010) 1294–1305.
[4] Y.Y. Xia, M. Yoshio, J. Electrochem. Soc. 144 (1997) 4186–4194.
[5] G. Amatucci, J.M. Tarascon, J. Electrochem. Soc. 149 (2002) K31–K46.
[6] H.W. Lee, P. Muralidharan, R. Ruffo, C.M. Mari, Y. Cui, D.K. Kim, Nano Lett. 10 (2010) 3852–3856.
[7] J.Y. Luo, H.M. Xiong, Y.Y. Xia, J. Phys. Chem. C 112 (2008) 12051–12057.
[8] J.Y. Luo, L. Cheng, Y.Y. Xia, Electrochem. Commun. 9 (2007) 1404–1409.
[9] X.L. Xiao, J. Lu, Y.D. Li, Nano Res. 3 (2010) 733–737.
[10] I. Taniguchi, N. Fukuda, M. Konarova, Powder Technol. 181 (2008) 228–236.
[11] D. Tonti, M.J. Torralvo, E. Enciso, I. Sobrados, J. Sanz, Chem. Mat. 20 (2008) 4783–4790.
[12] B.G. Park, S. Kim, I.D. Kim, Y.J. Park, J. Mater. Sci. 45 (2010) 3947–3953.
[13] T.F. Yi, X.G. Hu, C.S. Dai, K. Gao, J. Mater. Sci. 42 (2007) 3825–3830.
[14] I. Taniguchi, T. Yano, L.Q. Zhang, Kag. Kog. Ronbunshu 34 (2008) 594–597.
[15] C.H. Lu, S.W. Lin, J. Power Sources 97–98 (2001) 458–460.
[16] S.N. Polyakov, Tech. Phys. Lett. 37 (2011) 41–44.
[17] H.L. Zhu, Z.Y. Chen, S. Ji, V. Linkov, Solid State Ionics 179 (2008) 1788–1793.
[18] J.R. Ying, C.Y. Jiang, C.R. Wan, J. Power Sources 129 (2004) 264–269.
[19] K. Matsuda, I. Taniguchi, J. Power Sources 132 (2004) 156–160.
[20] C.H. Lu, T.Y. Wu, H.C. Wu, M.H. Yang, Z.Z. Guo, I. Taniguchi, Mater. Chem. Phys. 112 (2008) 115–119.
[21] J.B. Fei, Y. Cui, X.H. Yan, W. Qi, Y. Yang, K.W. Wang, Q. He, J.B. Li, Adv. Mater. 20 (2008) 452–456.
[22] Y.Y. Xia, H. Takeshige, H. Noguchi, M. Yoshio, J. Power Sources 56 (1995) 61–67.
[23] X.M. He, J.J. Li, Y. Cai, Y.W. Wang, J.R. Ying, C.Y. Jiang, C.R. Wan, J. Solid State Electrochem. 9 (2005) 438–444.
[24] S.B. Tang, M.O. Lai, L. Lu, Mater. Chem. Phys. 111 (2008) 149–153.
[25] X.C. Tang, X.W. Song, P.Z. Shen, D.Z. Jia, Electrochim. Acta 50 (2005) 5581–5587.
[26] W. Liu, G.C. Farrington, F. Chaput, B. Dunn, J. Electrochem. Soc. 143 (1996) 879–884.
[27] J.Y. Luo, Y.G. Wang, H.M. Xiong, Y.Y. Xia, Chem. Mat. 19 (2007) 4791–4795.
[28] D.K. Kim, P. Muralidharan, H.W. Lee, R. Ruffo, Y. Yang, C.K. Chan, H. Peng, R.A. Huggins, Y. Cui, Nano Lett. 8 (2008) 3948–3952.
[29] H.S. Carslaw, J.C. Jaeger, in: Conduction of Heat in Solid, Clarendon Press, Oxford, England, 1986, p. 233.
[30] X.C. Tang, L.Q. Li, B.Y. Huang, Y.H. He, Solid State Ionics 177 (2006) 687–690.
[31] X.Q. Wang, H. Nakamura, M. Yoshio, J. Power Sources 110 (2002) 19–26.
[32] L. Xiao, J.T. Lu, P.F. Liu, L. Zhuang, J. Phys. Chem. B 110 (2006) 2057–2063.